

行政院國家科學委員會專題研究計畫 成果報告

壓電傳感元件之波傳耦合層設計與元件整體之力電作用表現研究 研究成果報告(精簡版)

計畫類別：個別型
計畫編號：NSC 95-2221-E-002-116-
執行期間：95年08月01日至96年07月31日
執行單位：國立臺灣大學材料科學與工程學系暨研究所

計畫主持人：謝宗霖

計畫參與人員：博士班研究生：黃俊銘
碩士班研究生：柯忠廷
大學部專題生：連柏翰
協同研究人員：段維新教授、陳俊杉教授

報告附件：出席國際會議研究心得報告及發表論文

處理方式：本計畫可公開查詢

中華民國 96 年 10 月 23 日

壓電傳感元件之波傳耦合層設計與元件整體之
力電作用表現研究

計畫類別： 個別型計畫 整合型計畫
計畫編號：NSC 95-2221-E-002-116 -
執行期間：2006 年 8 月 1 日至 2007 年 7 月 31 日

計畫主持人：謝宗霖

共同主持人：

計畫參與人員：段維新教授(協同研究人員)、陳俊杉教授(協同研究人員)、碩博士班研究生與大學部專題生(共三名)

成果報告類型(依經費核定清單規定繳交)： 精簡報告 完整報告

本成果報告包括以下應繳交之附件：

- 赴國外出差或研習心得報告一份
- 赴大陸地區出差或研習心得報告一份
- 出席國際學術會議心得報告及發表之論文各一份
- 國際合作研究計畫國外研究報告書一份

處理方式：除產學合作研究計畫、提升產業技術及人才培育研究計畫、列管計畫及下列情形者外，得立即公開查詢

涉及專利或其他智慧財產權， 一年 二年後可公開查詢

執行單位：國立臺灣大學材料科學與工程學系暨研究所

中 華 民 國 96 年 10 月 23 日

Abstract

Ceramic-polymer composites are manufactured and studied for their applications in acoustic impedance matching. Various ceramic-epoxy composites are developed and their impedance properties studied. Among them, the zirconium oxide-epoxy composite exhibits a tolerable attenuation level and an optimum impedance value for matching the piezoelectric ceramic-water interface. It is then integrated on to a home-made medical high intensity focused ultrasound (HIFU) transducer to test its effectiveness. The beam profile of the HIFU transducer is characterized by a hydrophone, and an *in-vivo* experiment is carried out to gauge its performance.

Keywords: Acoustic matching layer; Ceramic-polymer composites; HIFU; *In-vivo* experiment

1. Introduction

Acoustic impedance describes the behaviours of acoustic waves traveling in substances, and is given by $Z = \rho \times c$, where ρ is density and c is acoustic wave velocity [1]. It plays an important role when one acoustic wave travels across the interface between two substances, the larger the impedance mismatch, the more the energy loss. Matching layer is a coating layer to abase the huge difference mismatch between two materials – piezoelectric PZT ceramic and water for example, where $Z_{PZT} = 35 \text{ MRayl}$ and $Z_{\text{water}} = 1.5 \text{ MRayl}$. However, the thickness of matching layers and their impedance values also affects the efficiency of power transmission. It can be shown that for a monochromatic plane wave, the maximum transmission between the PZT ceramic and water with impedances of Z_{PZT} and Z_{water} occurs for a matching layer of $\lambda_m/4$ thickness and of acoustic impedance Z_m , where:

$$Z_m = \sqrt{Z_{PZT} Z_{\text{water}}} \quad (1)$$

and λ_m is the wavelength in the matching layer material (see Fig.1) [2].

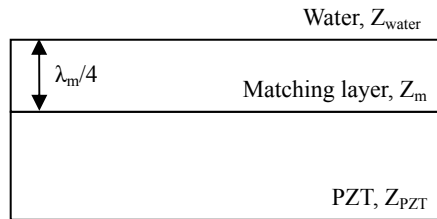


Fig. 1. Acoustic matching layer for PZT ceramic-water interface.

For acoustic matching applications, acoustic impedances of ceramic materials are too high for transmitting ultrasonic waves into water/human tissues. To reduce the

impedance, both the density and wave velocity within the ceramic need to be lower. Ceramic-polymer composites are potential matching layer materials capable of integrating into commercial transducers due to their modifiable impedances achieved by adjusting the volume percentages of components [3,4]. Due to the development of ultrasonic transducers of higher resonant frequencies for medical imaging applications, the required matching layer thickness becomes thinner, ranging from hundred nanometers to few micrometers. Therefore, for the homogeneity of the matching layer, the average ceramic particle size in ceramic-polymer composites is typically limited to nanometer size. Generally the impedances of ceramic-loaded epoxies range from 2.8 to 11.3 MRayl, depending on the material type and mixing ratio. Some existing studies have mentioned that the aging process of cured ceramic-epoxy composites can increase their impedances [5]. In the present study, various ceramic-epoxy composites are manufactured and studied for their applications in acoustic impedance matching.

2. Experimental procedure

In order to produce highly dense ceramic-epoxy composites, a new method involving the control of viscosity and bubble formation is adopted. The raw polymer and ceramic materials were two-part epoxy (Cheng-E Co., Taiwan), aluminum oxide powder (Al_2O_3 , Taimax Materials Co., Taiwan), zirconium oxide powder (ZrO_2 , Yageo Co., Japan), and barium titanate powder (BaTiO_3 , Yageo Co., Japan). The mean particle sizes were 223.5 nm, 1.619 μm , and 1.669 μm for ZrO_2 , Al_2O_3 , and BaTiO_3 , respectively. The powder size was characterized using a zeta potential meter (Zetasizer, Malvern Co., Taiwan).

The epoxy resin was pre-heated to 120°C and held for 10 minutes to lower its viscosity and release the residual bubbles. 20, 30, and 30 grams of Al_2O_3 , ZrO_2 , and BaTiO_3 powders were mixed separately with the pre-heated resin, respectively, to form colloidal solutions of volume 10 ml. The colloidal solutions were thoroughly stirred at 120°C and then placed in vacuum for 5 min for multiple times to ensure that the bubbles trapped between the ceramic particles escaped the colloidal solutions completely. The degree of compaction of the ceramic particles in the solutions gradually increased during the stir-then-vacuum procedure, and the resin eventually became excessive. The excess epoxy resin was removed, and the epoxy hardener was added into the solutions. Finally, the solutions were poured into wax molds and cured at room temperature for 24 hr. The resultant bulk composites were then aged at 80°C for 5 hr. The entire processing flow is schematically shown in Fig. 2.

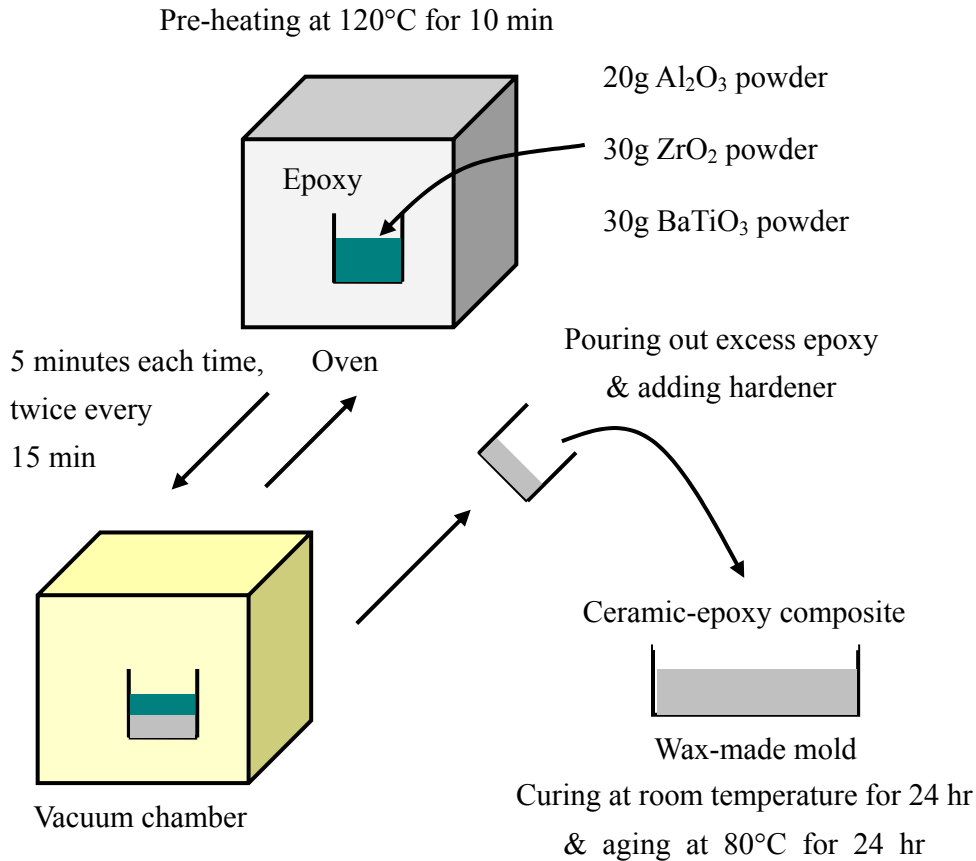


Fig. 2. Processing steps of acoustic matching composites.

To determine the acoustic impedance of a material, the wave traveling velocity in the material is a necessary parameter. Therefore, each of the prepared bulk ceramic-epoxy composite was cut and ground into a disc sample and adhered on to an ultrasonic probe (GE Panametrics Co., USA) using ultrasonic gel for wave velocity measurements. The ultrasonic probe was used to transmit and receive ultrasound waves under a pulser-receiver setup. The reflected wave signals were collected using an oscilloscope (Lecroy Co., USA). Recording the time interval between the reflected waves and knowing the sample thickness led to the value of wave velocity within the prepared composite matching layer.

In order to prevent frequency coupling between the transmitting and receiving waves within the ultrasonic probe, an external hydrophone (ONDA Co., Taiwan) was utilized to receive the acoustic waves emitting from the composite matching layer. The hydrophone measurement was set up under water to minimize attenuation and maximize the hydrophone efficiency. Each matching composite sample was set up identically on the ultrasonic probe as mentioned above. After traveling through the composite sample, the emitting ultrasonic waves were collected by the hydrophone

and then transformed into electrical signals to the oscilloscope. The measured wave forms were converted into frequency spectrums using Fast Fourier Transform (FFT). The measurement system for frequency distribution is shown in Fig. 3.

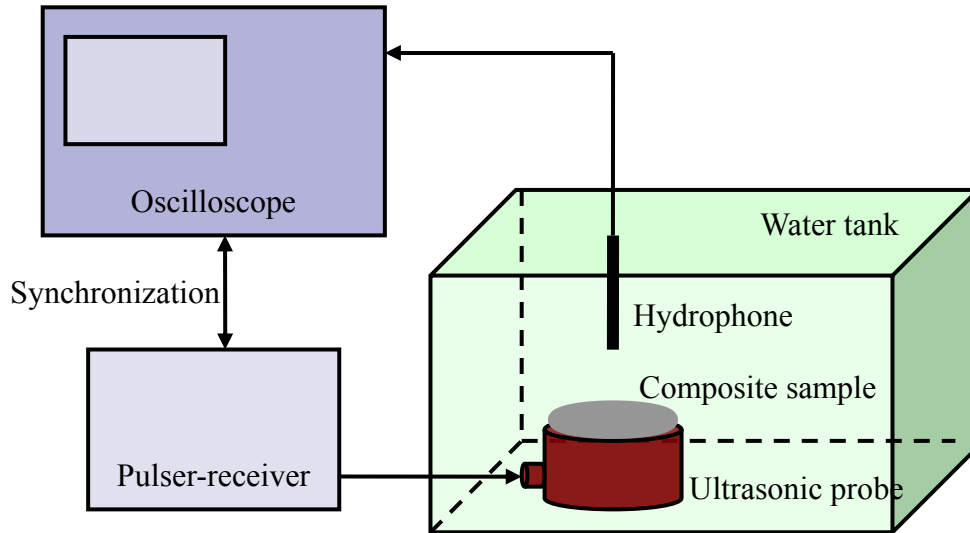


Fig. 3. Measurement system for frequency distribution of an ultrasonic transducer with a composite matching layer.

3. Measurements and discussion

The measured values of density, internal wave velocity, impedance, and attenuation of the three developed ceramic-epoxy composites are listed in Table 1. The internal wave velocity is calculated from the reflection time of 1 MHz wave traveling through a distance of double the thickness. A 180° phase shift at the composite-probe interface is discovered (i.e. a wave crest becomes a wave trough). It is found that the attenuation level of the epoxy increases when it is loaded with ceramic particles. This is due to the dissipation of acoustic energy at the ceramic-epoxy interfaces. Based on Eq. (1), a matching layer material with an impedance value close to 7 MRayl and of course low attenuation is desirable for transmitting ultrasonic waves from a ceramic piezoelectric transducer into water/human tissues. From Table 1, it is evident that ZrO₂-epoxy composite is the most suitable acoustic matching material due to its appropriate impedance value and reasonable attenuation.

In order to examine the acoustic matching efficiency of ZrO₂-epoxy composite, a quarter-wavelength ZrO₂-epoxy composite matching layer was integrated on to a home-made bowl-shape high intensity focused ultrasound (HIFU) transducer. The home-made HIFU transducer shown in Fig. 4 was manufactured to operate at 1.5

MHz. The bowl-shape piezoelectric (PZT) element of the transducer had a diameter of 10 cm and a curvature radius of 20 cm and was purchased from FUJI Ceramics Co., Japan. The electrical matching circuit of the transducer was built by BROADSOUND Co., Taiwan. The ultrasonic beam profiles of the transducer, such as the axial and lateral pressure distributions, were measured by a hydrophone moving incrementally along the axes by a step motor (see Fig. 5).

Composite	Density (g/cm ³)	Velocity (m/s)	Impedance (MRayl)	Attenuation (Np/cm)
Epoxy	1.162	2566.260	2.982	0.797
Al ₂ O ₃ -Epoxy	1.748	2835.081	4.956	0.916
ZrO ₂ -Epoxy	2.517	2503.831	6.302	0.973
BaTiO ₃ -Epoxy	2.633	2322.122	6.114	1.095

Table 1. Acoustic properties of developed composite materials.



Fig. 4. The home-made HIFU transducer with ZrO₂-epoxy matching layer.

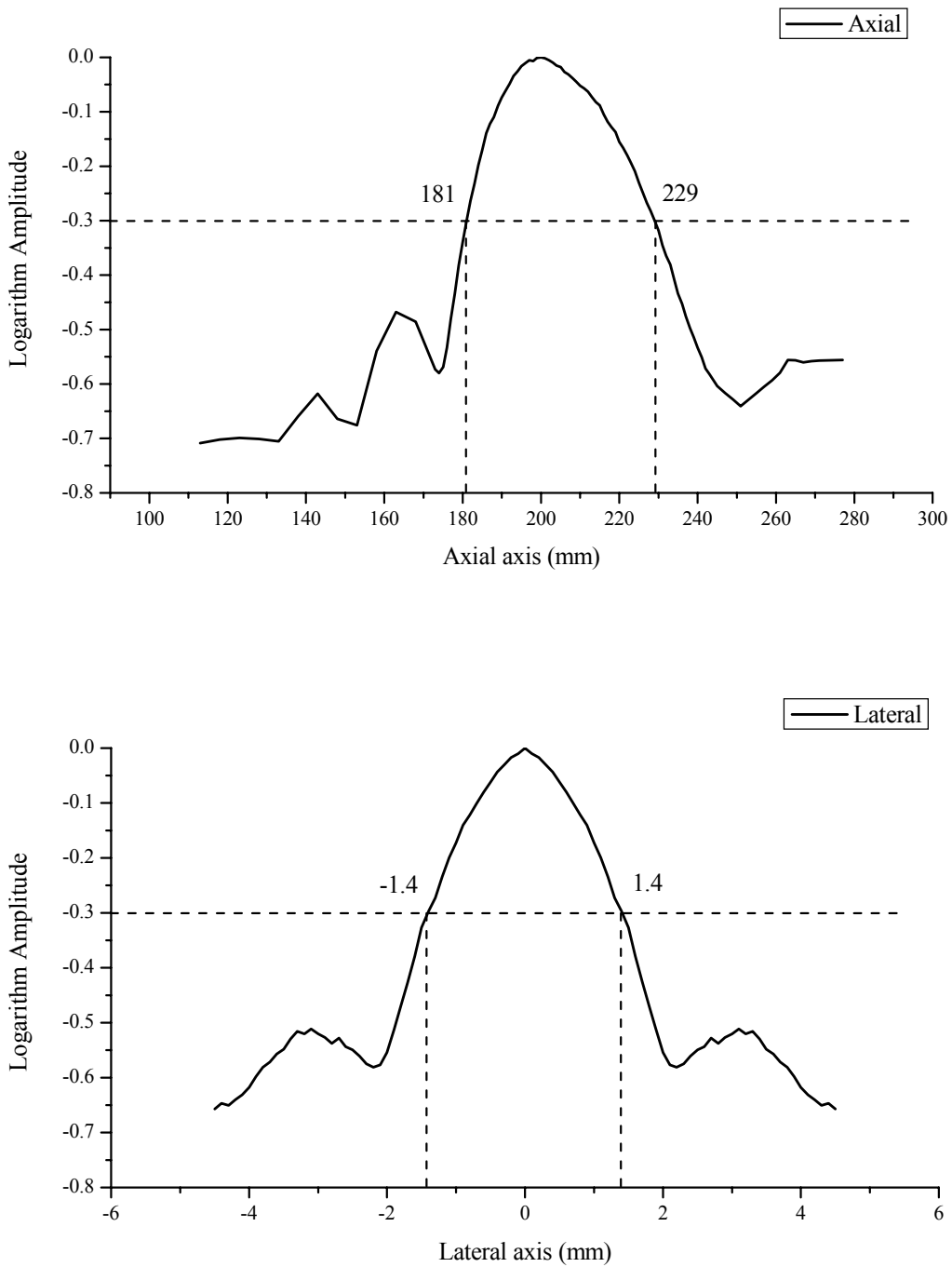


Fig. 5. Axial and lateral beam profiles of the home-made HIFU transducer.

An *in-vivo* experiment was carried out on a pork bulk to test the performance of the home-made HIFU. The experimental setup is shown in Fig 6. The pork bulk was pre-heated to 37°C to model the temperature of human tissues. The HIFU transducer is capable of driving at 105 watts with less than 2% power reflection.

The low level of power reflection demonstrates the high efficiencies of the acoustic and electrical matchings. After heating for 80 sec, the pork bulk was sliced into several pieces to measure the lesion size (shown in Fig. 7). The length and width of the lesion at the focal point were about 4.7 cm and 1.6 cm, respectively.

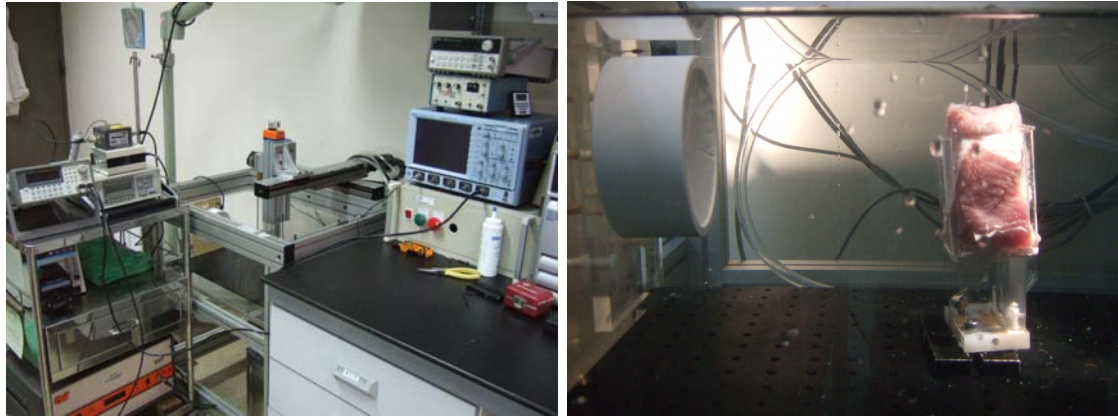


Fig. 6. Setup for *in-vivo* experiment.



Fig. 7. Lesion inside the pork bulk after *in-vivo* experiment.

4. Conclusion

In summary, three different ceramic-epoxy composites are developed and compared in terms of acoustic matching characteristics. Among them, ZrO_2 -epoxy composite is the most suitable material for matching layer applications due to its optimum acoustic impedance value for bridging the impedance mismatch between the ceramic piezoelectric element and water/human tissues. A bowl-shaped home-made HIFU transducer with a single ZrO_2 -epoxy composite matching layer is manufactured

to study the efficiency of the composite matching layer. The HIFU transducer could be driven at 105 watts with less than 2% power reflection. The performance of the HIFU transducer is demonstrated by an *in-vivo* experiment.

References

- [1] E. Tomas and G. Alvarez-Arenas, *IEEE Transactions on Ultrasonics, Ferroelectrics, and Frequency Control* **51**, 624 (2004).
- [2] L.E. Kinsler, A.R. Frey, A.B. Coppens, and J.V. Sanders, *Fundamentals of Acoustics*, 3rd Ed. (John Wiley, New York, 1982).
- [3] E. Yogeswaren, Matching Layer Assembly for a Downhole Acoustic Sensor, *US Patent*, No. **7075215**.
- [4] K. Hashimoto, T Hashida, M. Suzuki, M. Hashimoto, H. Nagahara, S. Shiraishi, and N. Takahara, Acoustic Matching Layer and Ultrasonic Transducer, *US Patent*, No. **6969943**.
- [5] H. Wang, W. Cao, Q. F. Zhou, K. K. Shung, and Y. H. Hung, *Applied Physics Letters* **85**, 5998 (2004).

計畫成果自評

With limited availabilities of time and funding, the acoustic matching characteristics of various ceramic-epoxy composites have been studied extensively. These composite materials have the potential to replace traditional polymer-based impedance matchings on commercial piezoelectric ultrasound transducers. A manuscript is currently under preparation for submission to international journals. Additionally, applications of ROC and US patents based on the findings of the present study are currently being processed. The contents of the patents are not discussed in the current report.

論文與專利之發表

1. J. Shieh, C.T. Ko, W.S. Chen, and C.S. Chen, Acoustic filtering behaviours of active PZT matching layers, manuscript in preparation.
2. J. Shieh, C.T. Ko, W.S. Chen, and C.S. Chen, Acoustic filtering by an active piezoelectric matching layer, ROC and US patents under application. (註：專利內容未在此報告內討論)

可供推廣之研發成果資料表

* 可申請專利

 可技術移轉

日期：96年10月23日

國科會補助計畫	計畫名稱：壓電傳感元件之波傳耦合層設計與元件整體之力電作用表現研究 計畫主持人：謝宗霖 計畫編號：NSC 95-2221-E-002-116 學門領域：金屬及陶瓷材料工程 (E8)
技術/創作名稱	一種可主動篩頻之波傳耦合層材料系統 (provisional)
發明人/創作人	謝宗霖 <i>et al.</i>
技術說明	Acoustic filtering by an active piezoelectric matching layer. (研發成果申請專利中，無法揭露專利內容)
可利用之產業 及 可開發之產品	電子陶瓷相關產業 超音波探頭相關產業 鐵電壓電元件
技術特點	主動篩頻
推廣及運用的價值	被動波傳耦合層之替代品

- ※ 1. 每項研發成果請填寫一式二份，一份隨成果報告送繳本會，一份送 貴單位研發成果推廣單位（如技術移轉中心）。
- ※ 2. 本項研發成果若尚未申請專利，請勿揭露可申請專利之主要內容。
- ※ 3. 本表若不敷使用，請自行影印使用。

出席國際學術會議心得報告

計畫編號	NSC 95-2221-E-002-116-
計畫名稱	壓電傳感元件之波傳耦合層設計與元件整體之力電作用表現研究
出國人員姓名 服務機關及職稱	謝宗霖助理教授, 國立臺灣大學材料科學與工程學系暨研究所
會議時間地點	San Diego, USA, 18-22 March 2007
會議名稱	SPIE's 14th International Symposium on Smart Structures and Materials and Nondestructive Evaluation and Health Monitoring
發表論文題目	Switching characteristics of $(\text{Bi}_{1/2}\text{Na}_{1/2})\text{TiO}_3\text{-BaTiO}_3\text{-(Bi}_{1/2}\text{K}_{1/2})\text{TiO}_3$ lead-free ferroelectric ceramics

一、參加會議經過及與會心得

The meeting at San Diego was a success. SPIE's annual meeting on smart materials and structures is one of the largest conferences in the world. International scholars and researchers in the field of ferroelectrics were very interested in the polarization and strain hysteresis measurements of the BNBK ceramics. There were lots of discussions on the processing, characterization, and possible applications of the lead-free BNBK ceramics. The depolarization temperature of BNBK was also a topic of high interest since this critical temperature point would decide how feasible the BNBK is used to replace lead-base ferroelectrics like the PZT family of ceramics. Overall, this was a highly productive and worthwhile conference trip. The conference proceeding (*Proc. of SPIE* Vol. **6526** 65260M) is attached below.

Switching characteristics of $(\text{Bi}_{1/2}\text{Na}_{1/2})\text{TiO}_3\text{-BaTiO}_3\text{-(Bi}_{1/2}\text{K}_{1/2})\text{TiO}_3$ lead-free ferroelectric ceramics

J. Shieh^{a*}, K.C. Wu^a, C.S. Chen^b

^aDepartment of Materials Science and Engineering

^bDepartment of Civil Engineering

National Taiwan University, 1 Roosevelt Road, Sec. 4, Taipei 106, Taiwan

ABSTRACT

The polarization switching characteristics of lead-free $a(\text{Bi}_{1/2}\text{Na}_{1/2})\text{TiO}_3\text{-}b\text{BaTiO}_3\text{-}c(\text{Bi}_{1/2}\text{K}_{1/2})\text{TiO}_3$ (abbreviated as BNBK 100*a*/100*b*/100*c*) ferroelectric ceramics are investigated. This is achieved through examining their polarization and strain hystereses inside and outside the morphotropic phase boundary (MPB). The total induced electrostrain ($\epsilon_{33,\text{total}}$) and apparent piezoelectric charge coefficient (d_{33}) first increase dramatically and then decrease gradually as the BNBK composition moves from the tetragonal phase to the MPB and then to the rhombohedral phase. The measured polarization hystereses indicate that the BNBK compositions situated near the rhombohedral side of the MPB typically possess higher coercive field (E_c) and remanent polarization (P_r), while the compositions situated near the tetragonal side of the MPB possess higher apparent permittivity. Adverse effects on the ferroelectric properties are observed when BNBK is doped with donor dopants such as La and Nb. On the contrary, intricate hysteresis behaviors are observed when acceptor dopant Mn is introduced into BNBK. Under an alternating electric field of $\pm 5.0 \text{ MVm}^{-1}$, BNBK 85.4/2.6/12, a composition well within the MPB, exhibits an $\epsilon_{33,\text{total}}$ of $\sim 0.14\%$, an apparent d_{33} of 295 pCn^{-1} , an E_c of 2.5 MVm^{-1} and a P_r of $22.5 \text{ } \mu\text{Ccm}^{-2}$. These notable ferroelectric property values suggest a candidate material for lead-free actuator applications. The present study provides a systematic set of hysteresis measurements which can be used to characterize the switching behaviors of BNBK-based lead-free ferroelectrics.

Keywords: BNBK, lead-free, ferroelectrics, ferroelectricity, hysteresis, polarization switching

* jayshieh@ntu.edu.tw; phone: +886-2-33665287; fax: +886-2-23634562

1. INTRODUCTION

There has been a determined effort to develop lead-free ferroelectric ceramics with high piezoelectric properties by various doping and alloying routes, but no effective alternative to the lead zirconate titanate (PZT) system has yet been found.¹ Nevertheless, several lead-free ceramic systems have shown great potential. Saito et al.² have developed a highly <001> textured alkaline niobate-based perovskite ceramic with a piezoelectric charge coefficient d_{33} of 416 pC/N⁻¹, which is widely regarded as the closest lead-free system to the actuator-grade hard and semi-hard PZT ceramics to date. A considerable literature also exists concerning the dielectric and piezoelectric properties of $(1-x)(\text{Bi}_{0.5}\text{Na}_{0.5})\text{TiO}_3$ - $x\text{BaTiO}_3$ (abbreviated as BNBT-100 x) and $(1-y)(\text{Bi}_{0.5}\text{Na}_{0.5})\text{TiO}_3$ - $y(\text{Bi}_{0.5}\text{K}_{0.5})\text{TiO}_3$ (abbreviated as BNKT-100 y) solid solutions.³⁻⁹ These two bismuth sodium titanate (BNT)-based ceramic solid solutions have rhombohedral-tetragonal morphotropic phase boundary (MPB) compositions existed on $x = 0.06$ - 0.07 for BNBT-100 x and $y = 0.16$ - 0.20 for BNKT-100 y .⁸⁻¹⁰ From these two solutions, a ternary system, $a(\text{Bi}_{0.5}\text{Na}_{0.5})\text{TiO}_3$ - $b\text{BaTiO}_3$ - $c(\text{Bi}_{0.5}\text{K}_{0.5})\text{TiO}_3$ (abbreviated as BNBK 100 $a/100b/100c$), can be developed.¹⁰ A piezoelectric charge coefficient of $d_{33} = 191$ pC/N⁻¹, an electromechanical coupling factor of $k_{33} = 0.56$ and a dielectric constant of $K_{33}^T = 1141$ have been observed for the BNBK 85.2/2.8/12 composition which has a tetragonal phase near the MPB.¹⁰ In comparison with BNBT and BNKT, compositions of the BNBK ternary system typically exhibit higher depolarization and/or Curie temperatures.^{5,10,11} So far the dielectric and piezoelectric properties of the BNBK system have received some limited attention.¹⁰⁻¹² However, there are no systematic data available on its polarization and strain hystereses. This insufficiency shall be addressed in the present study.

In broad terms, ferroelectric sensors operate within the linear regime with subsequent signal amplification: linearity is more important than signal power. In other applications such as ferroelectric actuators, nonlinear behavior is a consequence of operating at high power. Hence, it is critical to measure the polarization switching characteristics of a newly developed ferroelectric system in order to gauge its ability to be used as linear and/or nonlinear devices.¹³ The aim of this study is to investigate the switching characteristics of BNBK-based lead-free ferroelectric ceramics, focusing on the MPB compositions. This is achieved through examining their hystereses in the electric polarization (D) vs. electric field (E) and strain (ϵ) vs. electric field (E) responses.

2. EXPERIMENTAL PROCEDURE

Conventional mixed oxide techniques were used to prepare the BNBK ceramics. Reagent-grade metal oxide and carbonate powders were used as starting raw materials. These oxide and carbonate powders were mixed in ethanol and ball-milled for 24 h. After calcining (800 °C, 1 h), the powder mix was again ball-milled for 24 h with the addition of PVA binder. After the second ball-milling procedure, the ground ceramic powders were oven-dried (120 °C, 24 h) and then pressed into sample discs. After debinding (600 °C, 1 h), these sample discs were sintered at 1170 °C for 2 h in air. Crystalline phases of the sintered BNBK ceramic samples were confirmed using an X-ray diffractometer (Rigaku

D/max-B). In total, 11 types of BNBK composition samples were prepared and Fig. 1 shows their relative positions on the room temperature phase diagram of the $(\text{Bi}_{0.5}\text{Na}_{0.5})\text{TiO}_3$ - BaTiO_3 - $(\text{Bi}_{0.5}\text{K}_{0.5})\text{TiO}_3$ ternary system. Samples 1-9 situate within the MPB of BNBK and consist of 40 mol% BNBT and 60 mol% BNKT. The exact constitutions of the BNBT and BNKT components of a BNBK sample are expressed by the number affixed; for example, Sample 8, which is BNBK 6.5-20, is of composition 40 mol% $(\text{Bi}_{0.5}\text{Na}_{0.5})_{0.935}\text{Ba}_{0.065}\text{TiO}_3$ + 60 mol% $\text{Bi}_{0.5}(\text{Na}_{0.8}\text{K}_{0.2})_{0.5}\text{TiO}_3$. Note that Sample 8, BNBK 6.5-20, can also be denoted as BNBK 85.4/2.6/12 by working out the exact percentages of the three constituents, $(\text{Bi}_{0.5}\text{Na}_{0.5})\text{TiO}_3$, BaTiO_3 and $(\text{Bi}_{0.5}\text{K}_{0.5})\text{TiO}_3$. Sample 10 (i.e., BNBK 75/5/20) and Sample 11 (i.e., BNBK 90/5/5) are two compositions outside the MPB and situate at the tetragonal and rhombohedral regions, respectively. They do not lie on the 40 mol%-BNBT-60 mol%-BNKT composition line. Several MPB compositions of the BNBT and BNKT systems were also prepared via the same processing route in this study for comparison purposes. For polarization and strain hysteresis measurements, sample discs were cut into cuboidal specimens measuring $10 \times 10 \times 3$ mm and silver-based paints were applied onto the 10×10 mm faces to form top and bottom electrodes for electric field excitation. Electric field loading was applied using a high-voltage amplifier (Trek 20/20C), driven by a ferroelectric analyzer (aixACCT TF2000). The polarization and strain of the specimen during electrical loading were measured by the ferroelectric analyzer and miniature strain gauges (TML FBX-04-11-005LE) attached onto the 10×3 mm faces of the specimen, respectively. All hysteresis measurements were carried out at room temperature (~ 25 °C) with the specimen contained within a silicon oil bath to prevent electrical breakdown.

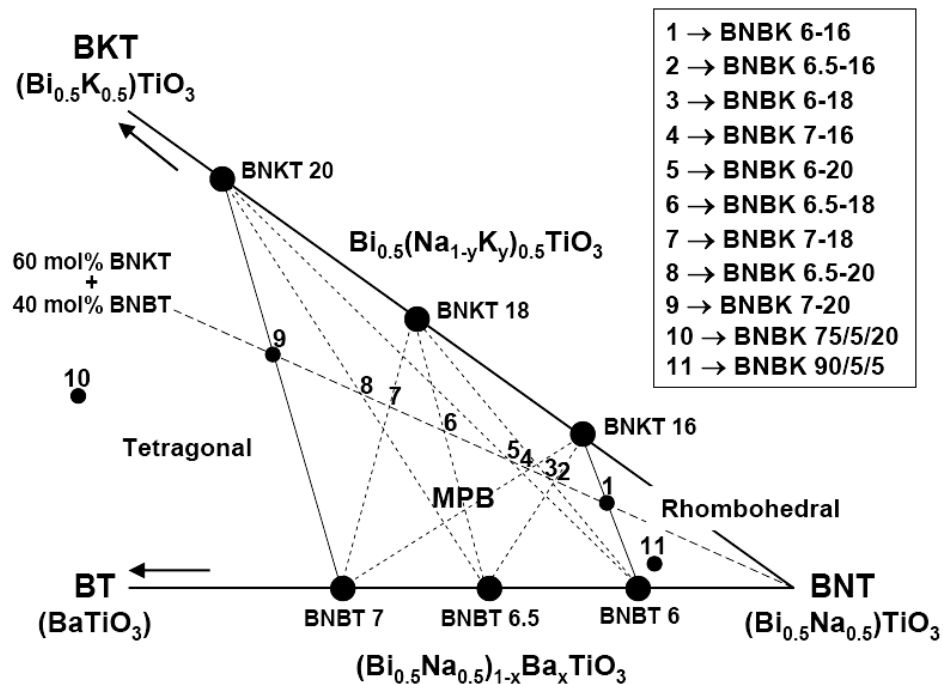


Fig. 1. Schematic of BNBK phase relationship around the MPB. Locations of 11 different BNBK composition samples prepared for the present study are shown.

3. MEASUREMENTS AND DISCUSSION

3.1 Polarization hysteresis

The stable polarization D - E hysteresis curves for the BNBK, BNBT and BNKT specimens, measured at a cyclic electric field of amplitude $\pm 5.0 \text{ MVm}^{-1}$, a frequency of 0.2 Hz and sinusoidal waveform, are shown in Fig. 2. The coercive fields (E_c) and remanent polarizations (P_r) of the specimens obtained from the measured D - E curves are listed in Table 1. It is evident from Fig. 2 that BNBT is the “softest” among the three ferroelectric systems, with its specimens showing the highest average P_r and lowest average E_c . In contrast, the BNKT specimens exhibit the lowest average P_r and a less sharp polarization transition at E_c (i.e., switching is completed over a wider range of electric field) – both are indications of a “hard” ferroelectric system. The switching behavior of BNBK in terms of hardness/softness falls in between the BNBT and BNKT systems and is strongly dependent on its composition. In all three systems, the specimens with compositions situated at or near the rhombohedral side of the MPB (e.g., BNBT-6, BNKT-16, BNBK 6-16, BNBK 6.5-16, BNBK 6-18 and BNBK 7-16) exhibit larger polarization hystereses, which typically give rise to higher E_c and P_r values, while the compositions situated at or near the tetragonal side of the MPB (e.g., BNBT-7, BNKT-20, BNBK 7-20 and BNBK 6.5-20) possess higher apparent permittivity, which could be calculated from the slope gradient of the D - E hysteresis curve at zero electric field. Among the nine MPB compositions of BNBK prepared for this study, BNBK 6.5-20 had the lowest E_c ($=2.5 \text{ MVm}^{-1}$) and BNBK 7-20 had a relatively high P_r ($=24.5 \text{ } \mu\text{Ccm}^{-2}$) with an E_c just below 3.0 MVm^{-1} .

3.2 Strain hysteresis

The stable strain ε - E hysteresis curves (i.e., butterfly curves) for the BNBK compositions inside and outside the MPB, measured at a cyclic electric field of amplitude ± 5.0 - 5.5 MVm^{-1} , a frequency of 0.2 Hz and sinusoidal waveform, are shown in Fig. 3. In order to achieve a satisfactory level of polarization saturation with 5.0 - 5.5 MVm^{-1} , only the BNBK compositions with $E_c < 3.0 \text{ MVm}^{-1}$ were chosen for the strain hysteresis analysis. Note that $\pm 15 \text{ kV}$ is needed to achieve $\pm 5.0 \text{ MVm}^{-1}$ on the 3 mm thick specimen. Strain measurements with excitation voltage $> 15 \text{ kV}$ were not carried out in order to protect the strain amplifier and gauges from high-voltage arc striking. It is evident from Fig. 3 that the tetragonal BNBK produces relatively the smallest strain under cyclic electrical loading. The remanent strain (ε_r) and total electrostrain in the 33-direction ($\varepsilon_{33,\text{total}}$) increase significantly when the BNBK composition moves from the tetragonal phase into the MPB, peaking at BNBK 6.5-20. While ε_r remains relatively unchanged, $\varepsilon_{33,\text{total}}$ decreases progressively as the composition shifts away from the MPB BNBK 6.5-20 into the rhombohedral phase, which is achieved by increasing the BNT amount in the BNBK system. Fig. 3 shows that MPB compositions BNBK 6.5-18 and BNBK 6-20, which contain more BNT than BNBK 6.5-20, exhibit smaller electrostrains. A similar trend to $\varepsilon_{33,\text{total}}$ is also observed for the apparent d_{33} , obtained from the slope gradient of the butterfly curve at zero electric field. With a composition well within the MPB, BNBK 6.5-20 exhibits an $\varepsilon_{33,\text{total}}$ of $\sim 0.14\%$, more than double than that of BNBK 7-20 which situates at the

tetragonal boundary of the MPB. The apparent d_{33} of BNBK 6.5-20 is 295 pC/V, an impressive number for a lead-free ferroelectric ceramic. The values of $\epsilon_{33, \text{total}}$ and apparent d_{33} for the chosen compositions are listed in Table 2.

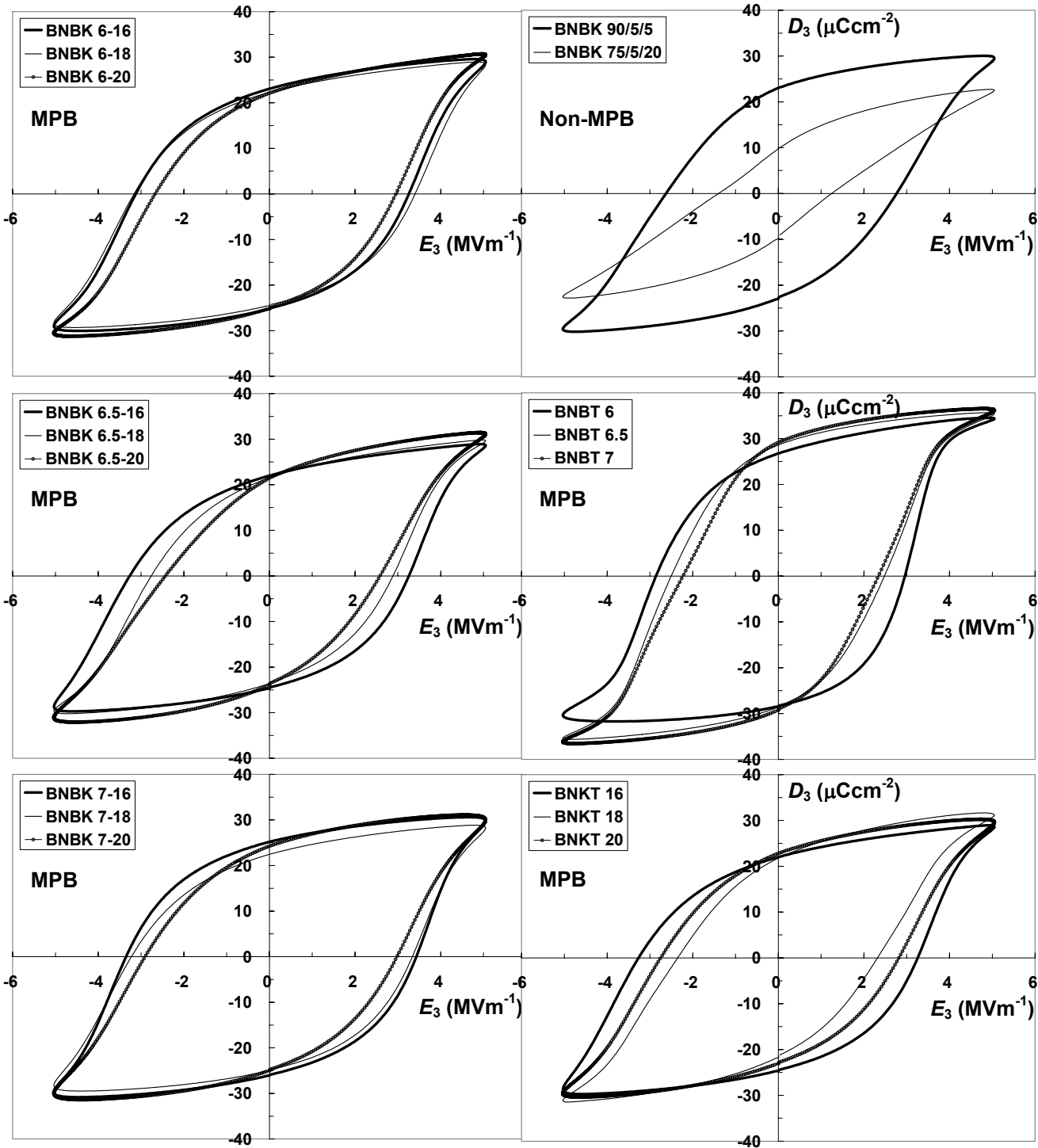


Fig. 2. Measured polarization D - E hysteresis curves for BNBK, BNBT and BNKT ($f_{\text{app}} = 0.2$ Hz).

Table 1. Coercive fields (E_c) and remanent polarizations (P_r) of BNBK, BNBT and BNKT compositions.

BNBK composition	P_r (μCcm^{-2})	E_c (MVm^{-1})	Composition	P_r (μCcm^{-2})	E_c (MVm^{-1})
6-16	24.0	3.2	BNBK 90/5/5	22.8	2.7
6-18	23.3	3.3	BNBK 75/5/20	9.5	1.3
6-20	23.4	2.8			
6.5-16	23.3	3.3	BNBT 6	27.4	2.9
6.5-18	22.5	2.8	BNBT 6.5	28.5	2.5
6.5-20	22.5	2.5	BNBT 7	29.1	2.3
7-16	25.5	3.4	BNKT 16	23.3	3.3
7-18	23.6	3.3	BNKT 18	21.6	2.3
7-20	24.5	3.0	BNKT 20	22.8	2.8

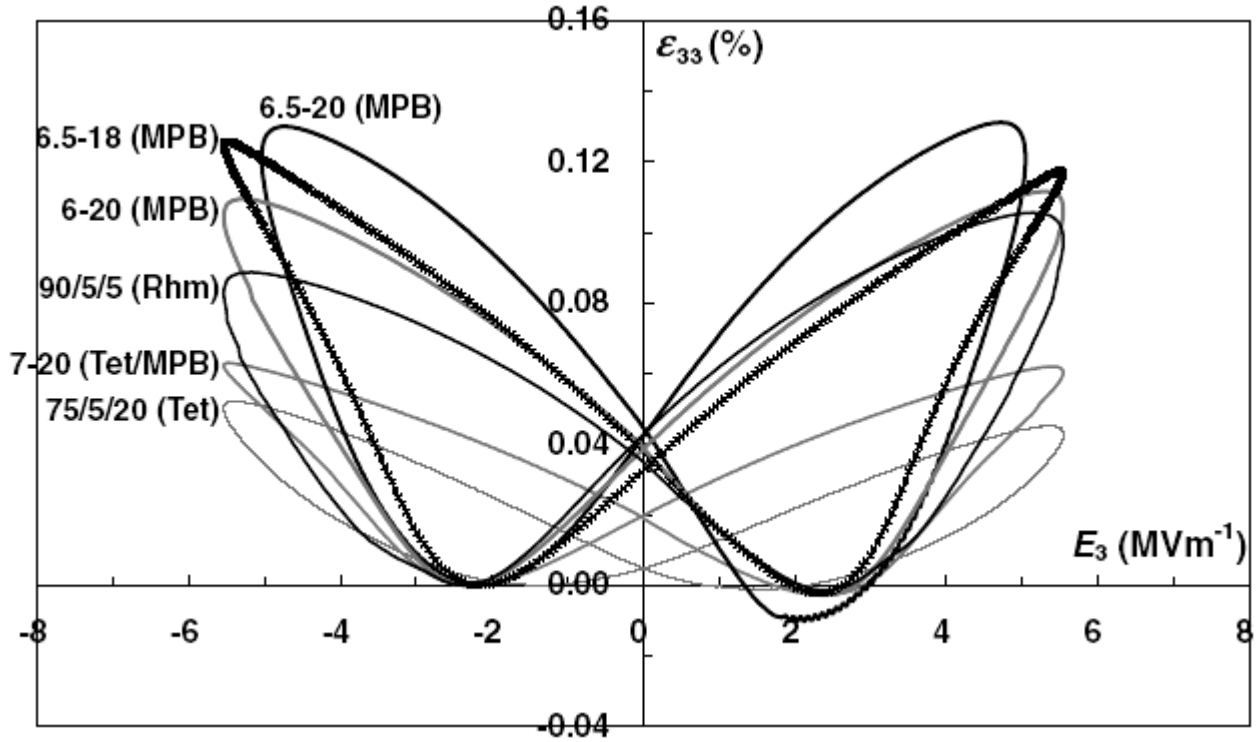


Fig. 3. Measured strain ε - E hysteresis curves for BNBK compositions inside and outside the MPB ($f_{\text{app}} = 0.2$ Hz).

The stable polarization and strain hysteresis curves for BNBK 90/5/5 and BNBK 75/5/20 are shown in Figs. 2 and 3, respectively. Apart from the actuating properties such as $\epsilon_{33,\text{total}}$ and d_{33} , the heavily BNT-based rhombohedral BNBK 90/5/5 also displays a much higher remanent polarization than the tetragonal BNBK 75/5/20. This is most likely due to the higher number of equivalent crystallographic directions which the spontaneous polarization could take up in a rhombohedral structure (i.e., eight [111] directions). Nevertheless, the magnitude of strain produced by BNBK 90/5/5 is still no match for those produced by the compositions well within the MPB. Fig. 4 compares the strain hystereses of BNBK 6.5-20 and its two constituent components, BNBT-6.5 and BNKT-20. A substantial 0.20% total electrostrain is observed for BNBT-6.5, a composition positioned right in the middle of the MPB of the BNBT system. When BNKT-20 is introduced into BNBT-6.5 (i.e., forming BNBK 6.5-20), decreases in the electrostrain and apparent d_{33} are obvious. This decline of actuating ability, though, is likely to be rewarded by increases in the depolarization and Curie temperatures (20-80 °C increase), as indicated by existing studies.^{5,10,11} The pure BNKT composition, BNKT-20, exhibits a small $\epsilon_{33,\text{total}}$ of ~0.05%, much less than those of BNBT-6.5 and BNBK 6.5-20. The values of $\epsilon_{33,\text{total}}$ and apparent d_{33} for BNBT-6.5 and BNKT-20 are also listed in Table 2. It is clear from Fig. 4 that the strain hysteresis of a BNBK composition combines the straining characteristics of its two constituent components, BNBT and BNKT.

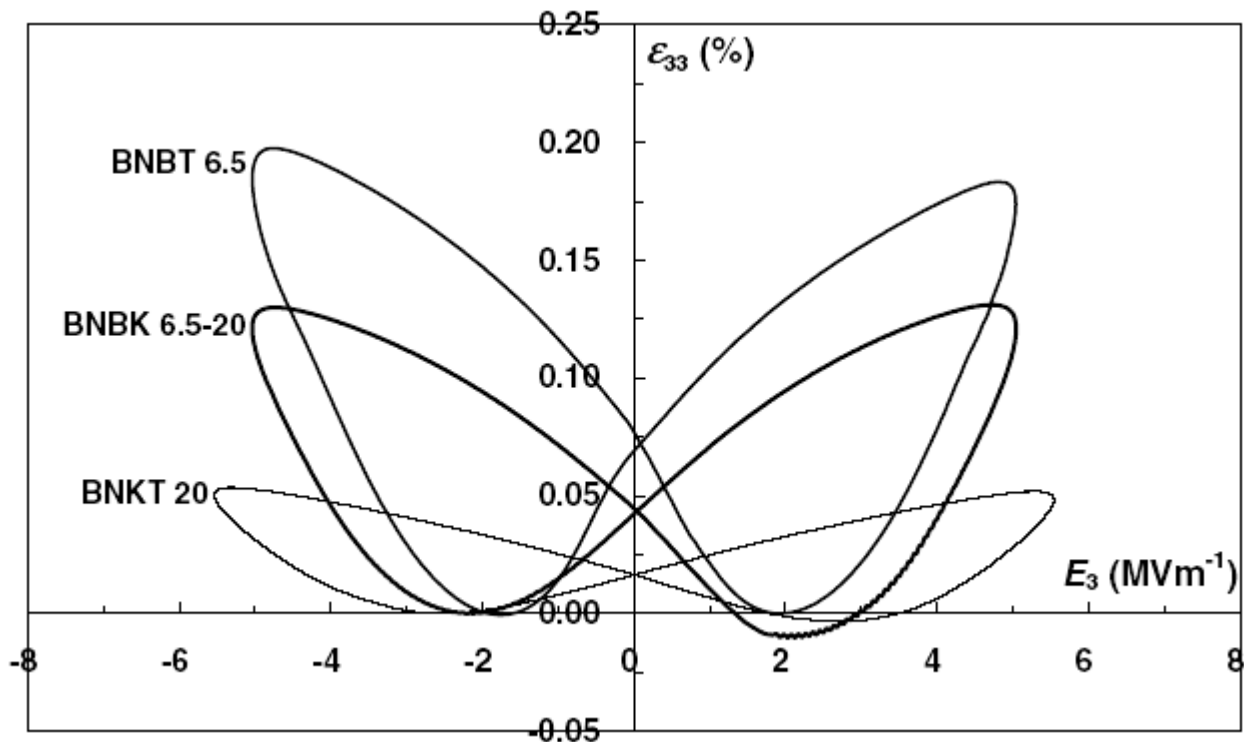


Fig. 4. Measured strain ϵ - E hysteresis curves for BNBT-6.5, BNKT-20 and BNBK 6.5-20 ($f_{\text{app}} = 0.2$ Hz).

Table 2. $\epsilon_{33,\text{total}}$ and apparent d_{33} of selected BNBK, BNBT and BNKT compositions.

BNBK composition	Crystallographic phase	$\epsilon_{33,\text{total}}$ (%)	Apparent d_{33} (pC/N ⁻¹)
75/5/20	Tetragonal	0.052	76
7-20	Tetragonal / MPB	0.064	121
6.5-20	MPB	0.140	295
6.5-18	MPB	0.126	216
6-20	MPB	0.114	209
90/5/5	Rhombohedral	0.107	205
Other composition			
BNBT 6.5	MPB	0.198	361
BNKT 20	Tetragonal / MPB	0.054	97

3.3 Doping effects

The stable polarization and strain hysteresis curves for BNBK 6.5-20 doped with 1.0 mol% La³⁺ and/or 1.0 mol% Nb⁵⁺ are shown in Fig. 5. Donor dopants for the PZT system such as La and Nb typically lower the coercivity and increase the polarization and actuation strain of PZT.¹⁴ However, it is evident from Fig. 5 that La and/or Nb dopings have adverse effects on the ferroelectric properties of the BNBK system. The magnitudes of induced polarization and strain decrease dramatically when La and/or Nb dopants are introduced into BNBK 6.5-20. This is likely due to the disappearance of large stable ferroelectric domains within the BNBK relaxor. In contrast, intricate hysteresis behaviors are observed when Mn, an acceptor dopant for the PZT system, is added into BNBK. The stable polarization and strain hysteresis curves for BNBK 6.5-20 doped with 0.1-2.9 mol% Mn²⁺ are shown in Fig. 6. It is evident that the apparent permittivity of BNBK 6.5-20 decreases with Mn doping and higher E_c and P_r values are measured when the Mn doping amount is higher than 1.0 mol%. $\epsilon_{33,\text{total}}$ of BNBK 6.5-20 decreases significantly when 0.1 mol% Mn²⁺ is added, but later recovers as the doping amount increases to 1.0 mol%. An asymmetric butterfly curve is observed when 2.9 mol% Mn²⁺ is added, which suggests a high degree of incomplete switching of polarization under an alternating electric field of ± 5.0 MVm⁻¹. This asymmetry is not observed in pure BNBK 6.5-20 and BNBK 6.5-20 doped with 0.1-1.0 mol% Mn²⁺ under an identical loading condition. Further detailed studies are required to explain the intricate hysteresis behaviors of Mn-doped BNBK.

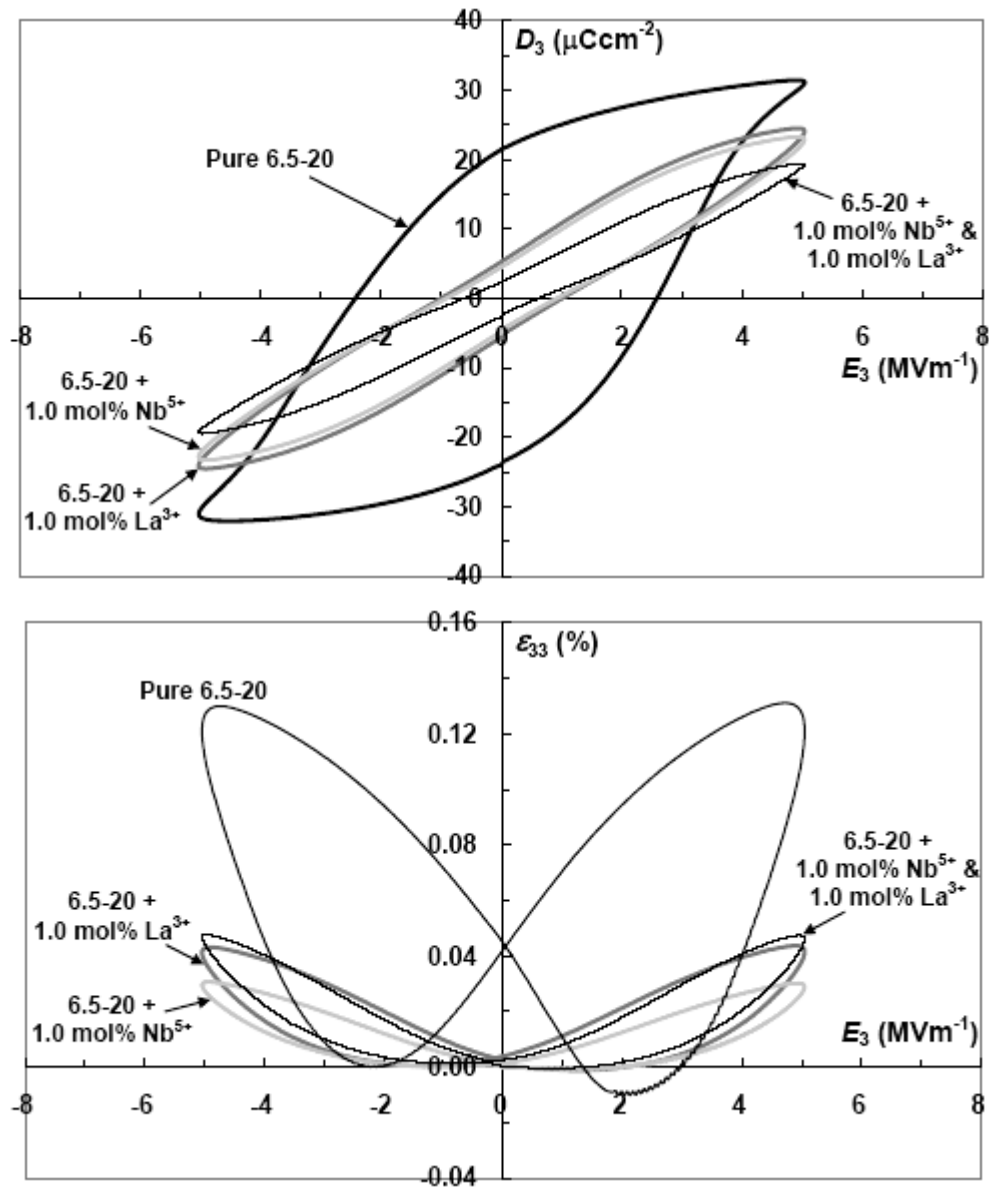


Fig. 5. Measured polarization and strain hysteresis curves for BNBK 6.5-20 doped with 1.0 mol% La^{3+} and/or 1.0 mol% Nb^{5+} .

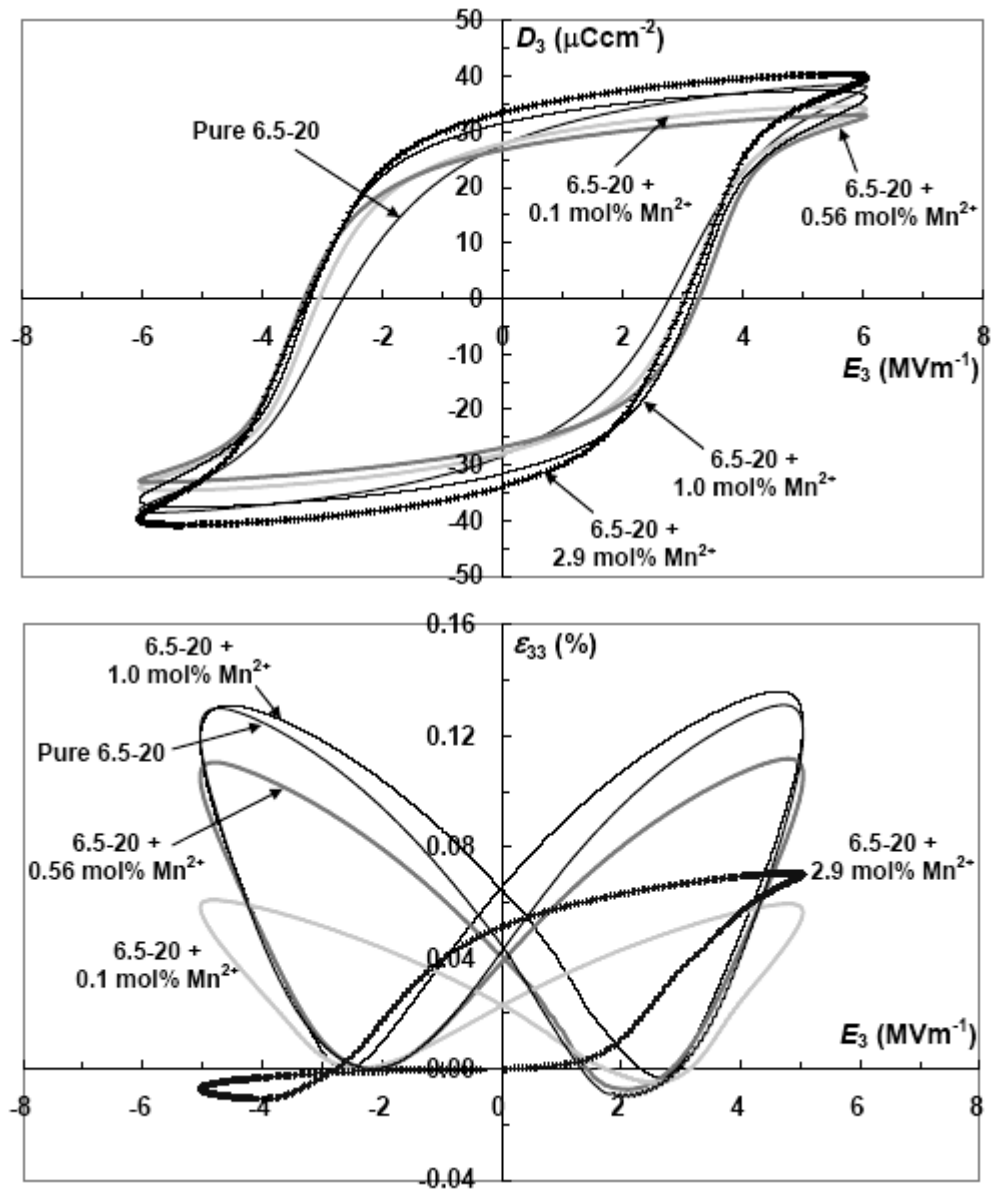


Fig. 6. Measured polarization and strain hysteresis curves for BNBK 6.5-20 doped with 0.1-2.9 mol% Mn²⁺.

4. CONCLUSION

In summary, the switching characteristics of the MPB compositions of the $(\text{Bi}_{0.5}\text{Na}_{0.5})\text{TiO}_3\text{-BaTiO}_3\text{-(Bi}_{0.5}\text{K}_{0.5})\text{TiO}_3$ lead-free system have been investigated. This was achieved through examining their polarization and strain hystereses. The BNBK compositions situated near the rhombohedral side of the MPB typically possess higher E_c and P_r , while the compositions situated near the tetragonal side of the MPB possess higher apparent permittivity. The total induced electrostrain and apparent d_{33} increase dramatically when the BNBK composition moves from the tetragonal phase into the MPB. They then decrease gradually as the composition shifts away from the MPB into the rhombohedral phase. Under an alternating electric field of $\pm 5.0 \text{ MVm}^{-1}$, BNBK 6.5-20 (a.k.a. BNBK 85.4/2.6/12) exhibits an $\epsilon_{33,\text{total}}$ of $\sim 0.14\%$, an apparent d_{33} of 295 pCn^{-1} , an E_c of 2.5 MVm^{-1} and a P_r of $22.5 \text{ } \mu\text{Ccm}^{-2}$. These notable ferroelectric property values indicate that the BNBK 6.5-20 ceramic is a candidate material for lead-free actuator applications.

ACKNOWLEDGEMENT

The authors are grateful for the financial support of the National Science Council (NSC) of Taiwan under contract numbers NSC94-2218-E-002-062 and NSC94-2216-E-002-019.

REFERENCES

1. Takenaka T, Nagata H. J Eur Ceram Soc 2005;25:2693.
2. Saito Y, Takao H, Tani T, Nonoyama T, Takatori K, Homma T, Nagaya T, Nakamura M. Nature 2004;432:84.
3. Kundu A, Soukhojak AN. Appl Phys A 2006;82:309.
4. Qu Y, Shan D, Song J. Mater Sci Eng B 2005;121:148.
5. Wang XX, Or SW, Tang XG, Chan HLW, Choy PK, Liu PCK. Solid State Commun 2005;134:659.
6. Wang XX, Kwok KW, Tang XG, Chan HLW, Choy CL. Solid State Commun 2004;129:319.
7. Ishii H, Nagata H, Takenaka T. Jpn J Appl Phys 2001;40:5660.
8. Sasaki A, Chiba T, Mamiya Y, Otsuki E. Jpn J Appl Phys 1999;38:5564.
9. Takenaka T, Maruyama K, Sakata K. Jpn J Appl Phys 1991;30:2236.
10. Nagata H, Yoshida M, Makiuchi Y, Takenaka T. Jpn J Appl Phys 2003;42:7401.
11. Wang XX, Choy SH, Tang XG, Chan HLW. J Appl Phys 2005;97:104101.
12. Wang XX, Tang XG, Chan HLW. Appl Phys Lett 2004;85:91.
13. Shieh J, Huber JE, Fleck NA. Acta Mater 2003;51:6123.
14. Moulson AJ, Herbert JM. Electroceramics: Materials, Properties and Applications. London: Chapman & Hall; 1990.